

1 **Blood-based near-infrared spectroscopy for the rapid low-cost detection of**
2 **Alzheimer's disease**

3 Maria Paraskevasidi^{1,*}, Camilo L. M. Morais¹, Daniel L. D. Freitas², Kássio M. G. Lima², David
4 M. A. Mann³, David Allsop⁴, Pierre L. Martin-Hirsch⁵, Francis L. Martin^{1,*}

5 *¹School of Pharmacy and Biomedical Sciences, University of Central Lancashire, Preston*
6 *PR1 2HE, UK*

7 *²Institute of Chemistry, Biological Chemistry and Chemometrics, Federal University of Rio*
8 *Grande do Norte, Natal 59072-970, Brazil*

9 *³Clinical Neuroscience Research Group, Division of Medicine and Neuroscience, University*
10 *of Manchester, Greater Manchester Neurosciences Centre, Hope Hospital, Salford M6 8HD,*
11 *UK*

12 *⁴Division of Biomedical and Life Sciences, Faculty of Health and Medicine, Lancaster*
13 *University, Lancaster LA1 4YQ, UK*

14 *⁵Department of Obstetrics and Gynaecology, Central Lancashire Teaching Hospitals NHS*
15 *Foundation Trust, Preston PR2 9HT, UK*

16

17

18

19

20

21

22

23

24

25

26

27

28

29 ¹To whom correspondence should be addressed. Email: mparaskevasidi@uclan.ac.uk or
30 flmartin@uclan.ac.uk

31 **Abstract**

32

33 Alzheimer's disease (AD) is currently under-diagnosed and is predicted to affect a great
34 number of people in the future, due to the unrestrained aging of the population. An accurate
35 diagnosis of AD at an early-stage, prior to (severe) symptomatology, is of crucial importance
36 as it would allow the subscription of effective palliative care and/or enrolment into specific
37 clinical trials. Today, new analytical methods and research initiatives are being developed for
38 the on-time diagnosis of this devastating disorder. During the last decade, spectroscopic
39 techniques have shown great promise in the robust diagnosis of various pathologies, including
40 neurodegenerative diseases and dementia. In the current study, blood plasma samples were
41 analysed with near-infrared (NIR) spectroscopy as a minimally-invasive method to distinguish
42 patients with AD ($n=111$) from non-demented volunteers ($n=173$). After applying multivariate
43 classification models (principal component analysis with quadratic discriminant analysis –
44 PCA-QDA), AD individuals were correctly identified with 92.8% accuracy, 87.5% sensitivity
45 and 96.1% specificity. Our results show the potential of NIR spectroscopy as a simple and cost-
46 effective diagnostic tool for AD. Robust and early diagnosis may be a first step towards
47 tackling this disease by allowing timely intervention.

48

49

50

51

52

53 **Keywords:** Alzheimer's disease; multivariate classification; near infrared spectroscopy; PCA-
54 QDA; plasma diagnostics

55 **Introduction**

56 Alzheimer's disease (AD), being responsible for 60-80% of the cases, constitutes the
57 most common type of dementia. A risk factor for the development of AD is increasing age,
58 which, in combination with the progressive increase in the number of elderly people, is
59 expected to lead to ~135 million affected individuals worldwide by 2050 ¹. Apart from the
60 detrimental impact of this disorder on patients, their families and the society, the economic
61 burden should also be considered; the worldwide cost had been estimated to become a US\$
62 trillion dollar disease in 2018 ². Furthermore, AD is definitively diagnosed only after a post-
63 mortem brain biopsy. It is therefore more than evident that effective means to diagnose AD
64 accurately and at an early-stage is crucial in order to intervene with therapeutic strategies and
65 recruit patients to clinical trials.

66 Infrared (IR) spectroscopy has advanced significantly over the last decades, specifically
67 in the field of biomedical investigation ^{3, 4}. By exploiting the vibrational movements of the
68 chemical bonds within a sample after excitation, IR spectroscopy can provide quantitative and
69 qualitative information about a sample. Technological advancements have also simplified the
70 previously expensive and complicated instrumentation, thus facilitating the wider-use of these
71 systems. In this study, near-IR (NIR) spectroscopy was employed to study the region of the
72 electromagnetic spectrum ranging between ~750-2500 nm. The most prominent bands in the
73 NIR include overtones and combinations of fundamental vibrations of -CH, -NH, -OH groups
74 ⁵. It has been previously shown that NIR spectroscopy holds promise for biomedical
75 applications ⁶, including the study of human skin (skin carcinomas, atopy and leprosy) ⁷,
76 diabetes ⁸, breast and colorectal cancers ^{9, 10}, Alzheimer's disease ¹¹ and chronic fatigue
77 syndrome ¹².

78 Spectroscopic techniques have been previously employed by independent research
79 groups for the investigation of neurodegenerative disorders, either by analysis of brain biopsies

80 or biofluids, such as cerebrospinal fluid (CSF) and blood samples¹³⁻¹⁷. The objective of the
81 current study was to detect AD using a minimally-invasive, but at the same time rapid and
82 inexpensive, blood test. Our aim was to use a large number of individuals and add further
83 evidence, to the current literature, about the diagnostic capabilities of spectroscopy as a
84 diagnostic tool.

85 The use of a suitable substrate in spectroscopy is also of major importance as it could
86 distort the resultant spectral information and lead to falsified conclusions; for this reason,
87 numerous studies have previously used costly and/or fragile substrates, such as calcium/barium
88 fluoride or gold substrates, to avoid signal interference¹⁸⁻²². At the same time, however, the
89 substrate of choice should be relatively inexpensive in order to be welcomed to a clinical
90 setting. Therefore, a secondary aim of this study was to investigate whether the signal from the
91 commonly-used and inexpensive low-E glass slide^{23,24} could be removed from the samples'
92 spectra without affecting the diagnostic result.

93 **Materials and Methods**

94 **Patient cohort and sample collection**

95 Our cohort included 111 patients with AD and 173 individuals with no symptoms of
96 AD, who were designated as healthy controls (HC). The latter group mainly consisted of close
97 relatives (*e.g.*, spouses) escorting the patients at the time of examination. More information
98 about the age and gender of the participants is provided in Table 1.

99 All participants were recruited at Salford Royal Hospital (Salford, UK) with informed
100 consent obtained prior to enrolment in accordance with Local Ethical Approval (05/Q1405/24
101 conferred by North West 10 Research Ethics Committee Greater Manchester North). Blood
102 samples were collected in EDTA tubes following standard operating procedures. To acquire
103 the plasma, whole blood was centrifuged for 10 min at 2000 rpm, 4°C and the supernatant was

104 collected in new microtubes. Plasma samples were aliquoted and kept at -80°C until needed for
105 the spectroscopic analysis. Samples were thoroughly thawed before depositing 50 µL onto IR-
106 reflective glass slides (MirrIR Low-E slides, Kevley Technologies, USA) and left to dry
107 overnight at room temperature.

108 **NIR spectroscopy**

109 Spectra were acquired using an ARCoptix FT-NIR Rocket spectrometer (Arcoptix
110 S.A., Switzerland) in the range of 900 to 2600 nm. Samples were interrogated using the
111 transmission mode with 10 point spectra collected per sample (resolution of 8 cm⁻¹). Each
112 sample spectrum was subtracted by a low-E slide background spectrum in order to eliminate
113 the signal resulting from the slide.

114 **Pre-processing and computational analysis**

115 Data pre-processing and multivariate classification models were built using MATLAB
116 R2014b software (MathWorks Inc., USA) with PLS Toolbox version 7.9.3 (Eigenvector
117 Research Inc., USA) and lab-made routines. The 10 spectra collected per sample were initially
118 averaged, and the following pre-processing steps were applied to the dataset: truncation at the
119 biofingerprint region (1850-2150 nm) (highlighted in Fig. 1a), Savitzky-Golay (SG) smoothing
120 to remove unwanted noise from the spectra (window = 15 points, 2nd order polynomial
121 function), extended multiplicative signal correction (EMSC) to correct for light scattering and
122 automatic weighted least squares baseline correction to remove baseline absorptions. The
123 spectra were divided into training (70%) and test (30%) sets using the Kennard-Stone (KS)
124 sample selection algorithm²⁵. The training set was used for construction of the classification
125 models, whereas the test set was only used for final model evaluation.

126 Classification was performed using principal component analysis with quadratic
127 discriminant analysis (PCA-QDA). PCA-QDA model is based on a PCA decomposition

128 followed by a Mahalanobis distance calculation. PCA reduces the original dataset into a few
129 number of principal components (PCs) accounting for the majority of the variance across the
130 spectra. As a result, a scores and a loading array are generated for each PC representing the
131 variance on the sample and variable (*e.g.*, wavelength) directions, respectively ²⁶. PCA also
132 solves problems with ill-conditioned data (data matrix with large condition number) by
133 reducing redundant information across the data and solving collinearity problems. For this
134 reason, PCA is commonly employed prior to discriminant analysis, with the PCA scores used
135 as input variables for the QDA algorithm.

136 As aforementioned, QDA is a classification algorithm based on a Mahalanobis distance
137 calculation. QDA assumes classes having different variance structures, calculating an
138 individual variance-covariance matrix for each class ²⁷. This improves the classification
139 capacity of QDA in comparison to linear methods (*e.g.*, linear discriminant analysis – LDA)
140 when classes with different variances are being analysed, which occurs often in complex
141 datasets. The QDA classification scores were calculated in a non-Bayesian form in order to
142 reduce the degree of overfitting, as follows ²⁸:

$$143 \quad Q_{ik} = (\mathbf{x}_i - \bar{\mathbf{x}}_k)^T \mathbf{C}_k^{-1} (\mathbf{x}_i - \bar{\mathbf{x}}_k) \quad (01)$$

144 where Q_{ik} is the QDA classification score for sample i of class k ; \mathbf{x}_i is the vector containing
145 the classification variables for sample i (*i.e.*, PCA scores); $\bar{\mathbf{x}}_k$ is the mean vector for class k ;
146 \mathbf{C}_k is the variance-covariance matrix of class k ; and T represents the transpose matrix.

147 Outliers were identified using a Hotelling T^2 versus Q residual test ²⁹. This test enables someone
148 to create a chart containing the Hotelling T^2 values in the x-axis and the Q residuals in the y-
149 axis, where all samples far from the origin [0,0] are considered to be outliers. The Hotelling T^2
150 values represent the sum of the normalised PCA scores, which is the distance from the
151 multivariate mean to the projection of the sample onto the PCs; and the Q residuals are the sum

152 of squares of each sample in the error matrix, which are the residuals between the sample and
153 its projection *via* PCA.

154 **Model validation**

155 Validation was performed on a patient basis, meaning that each sample represents a
156 different patient rather than an individual spectrum. The models were validated using quality
157 parameters including accuracy (total number of samples correctly classified considering true
158 and false negatives), sensitivity (proportion of positives correctly identified), specificity
159 (proportion of negatives correctly identified), positive predictive value (proportion of test
160 positives which are true positives) and negative predictive value (proportion of test negatives
161 which are true negatives) (Table S1) ³⁰.

162 In addition, receiver operating characteristics (ROC) curve was generated using
163 easyROC version 1.3 (<http://www.biosoft.hacettepe.edu.tr/easyROC/>) ³¹, where area under the
164 curve (AUC) value was calculated as a general indicator of how well the model distinguished
165 between the classes.

166 **Results**

167 In total, we acquired 1110 NIR spectra from AD patients ($n=111$) and 1730 spectra
168 from HC volunteers ($n=173$). The absorption due to the low-E slide signal was subtracted from
169 the samples' signal in order to reduce glass interference (Figure S1). The average raw and pre-
170 processed spectra (truncation at 1850-2150 nm, SG smoothing, EMSC and baseline correction)
171 for each class are depicted in Figure 1. Seven outliers (three due to AD and four due to HC
172 samples) were detected using a Hotelling T^2 versus Q residual test (Figure S2). These samples
173 were removed from the classification model. In total, 194 samples were used in the training set
174 (118 HC, 76 AD) and 83 samples in the test set (51 HC, 32 AD), defined by the KS algorithm.
175 After pre-processing, slight visual differences are evident between HC and AD patients (Figure

176 1b). Significant differences were observed between HC and AD spectra (1850-2150 nm) using
177 a two-tailed *t*-test with 95% confidence level ($p < 0.001$).

178 For classification, the PCA-QDA algorithm was applied using 2 PCs (67.24%
179 cumulative explained variance). PCA scores and loadings are depicted in Figure 2a and 2b,
180 respectively. The scores profile on the two PCs were superposed for HC and AD samples, with
181 no clear separation observed between the classes. The loadings profiles (Figure 2b) indicated
182 greater differences close to regions corresponding to a combination of O-H stretch/C-O stretch
183 second overtone (~1860 nm); second overtone C=O stretching (H-bonded) in peptides (1908
184 nm); and a combination of bands consisting of N-H bend second overtone, C-H stretch/C=O
185 stretch, C=O stretch/N-H in-plane bend/C-N stretching in proteins (2100 nm, 2111 nm, 2150
186 nm) ³²⁻³⁴. These bands correspond to the most important spectral features used by the QDA
187 classifier in PCA-QDA. The PCA-QDA model distinguished between AD and HC individuals
188 with 92.8% accuracy, 87.5% sensitivity and 96.1% specificity (Table 2). The ROC curve and
189 AUC value for PCA-QDA are shown in Figure 3. The AUC value (0.928) is close to the
190 maximum of 1, indicating its excellent predictive response.

191 **Discussion**

192 With improved life conditions and health care, increased longevity has resulted into a
193 greater number of elderly people and, thus, many cases of demented individuals worldwide.
194 Numerous research groups have devoted substantial resources and co-ordinated their efforts to
195 study dementias and provide an accurate diagnosis. For instance, the most studied biomarkers
196 for AD are amyloid- β ($A\beta$) and tau protein (phosphorylated-tau and total-tau) in CSF.
197 Collection of CSF, however, is an invasive procedure, rendering routine testing difficult. The
198 understanding that the blood-brain barrier (BBB) is a semipermeable membrane, allowing the
199 secretion of biological molecules between brain and peripheral blood, as well as the fact that

200 500 mL CSF is daily absorbed into the bloodstream, has led to the characterization of blood as
201 an “information-rich” sample ³⁵.

202 Blood biomarkers indicative of disease constitute a developing field with great promise
203 in the area of neurodegenerative disorders. A great number of new, blood-based molecular tests
204 have emerged over the years, suggesting different biological markers for the detection of AD
205 and other dementias ³⁵⁻⁴¹. Even though the diagnostic capability of the above-mentioned tests
206 is satisfactory, the high cost and laborious experimental work of these methods are great
207 disadvantages for the development of a clinical test.

208 In contrast to conventional molecular techniques, spectroscopic tests allow cost-
209 effective and rapid results. Previous studies using the mid-IR region for the diagnosis of AD
210 have achieved comparable diagnostic results with the current NIR study. For instance, using
211 ATR-FTIR in the mid-IR region, Paraskevaidi et al. achieved 86% sensitivity and specificity
212 for individuals who carried one or two alleles of apolipoprotein e4 (*APOE* ϵ 4) ⁴²; Carmona et
213 al. used the mid-IR (as well as Raman spectroscopy) to differentiate between healthy elderly
214 and demented patients with a sensitivity of 89% and specificity of 92% ¹⁴; Peuchant et al. also
215 employed mid-IR spectroscopy and achieved 98.4% diagnostic accuracy ⁴³. Other preliminary
216 studies, have also successfully applied spectroscopic approaches (IR or Raman spectroscopy)
217 for the diagnosis of AD or other types of dementia ^{15, 44, 45}; however, the small number of
218 samples in these studies was a limitation, preventing more general conclusions. According to
219 the NIR results of the present study, most of the differences between healthy and demented
220 individuals seem to be related mainly to protein bands. Some of the well-known characteristics
221 of AD include the built-up of A β plaques and neurofibrillary tangles (primarily consisting of
222 tau protein) in the brain, and therefore we can speculate that the observed changes in the NIR
223 region may be attributed to such protein changes.

224 The current study has achieved exceptionally high diagnostic accuracies using NIR
225 spectroscopy in the transmission mode. The PCA-QDA classification model presented 92.8%
226 accuracy, 87.5% sensitivity and 96.7% specificity which are comparable, and even superior, to
227 current conventional diagnostic biomarkers. Using NIR spectroscopy, also decreases the
228 instrumental cost substantially, as instrumentation is much cheaper than other IR or Raman
229 systems and it can be easily translated to portable systems. Our results, coming from a large
230 cohort, add to the current literature by validating previous spectroscopic work, thus taking
231 spectroscopy one step forward towards clinical implementation. Indeed, repetition and
232 validation in independent research groups is of crucial importance for every new biomarker or
233 diagnostic test prior to clinical trials. Herein, we have also shown that after appropriate spectral
234 pre-processing, the low-E signal can be subtracted from the spectra, therefore allowing direct
235 comparison of the sample information without interference from the slide. It should be noted
236 here that the patient cohort in this study was already diagnosed with the disease, therefore the
237 potential of blood-based NIR spectroscopy for pre-symptomatic detection remains to be further
238 explored. Nevertheless, we are optimistic as previous spectroscopy studies have demonstrated
239 segregation between early-stage/mild AD and healthy controls^{15, 44, 46}, but a larger number of
240 early-stage patients is still required.

241 To conclude, this study detected a blood signature for AD, showing great promise in
242 the accurate, simple and minimally-invasive diagnosis of the disease. Our main objective in
243 the current study was to show whether NIR spectroscopy, in the transmission mode, could
244 provide satisfactory diagnostic performance after removal of the substrate's signal. Future
245 studies should focus on the recruitment of more participants, including asymptomatic
246 individuals or patients with mild cognitive impairment (MCI). This would be the next big step
247 in this field, as accurate identification of MCI individuals would allow immediate management

248 and recruitment into clinical trials; the latter may also prove crucial for the development of new
249 therapeutic strategies.

250 **Acknowledgments**

251 MP acknowledges Rosemere Cancer Foundation for funding. CLMM would like to thank
252 CAPES-Brazil (Doutorado Pleno no Exterior, grant 88881.128982/2016-01) for financial
253 support. KMGL would like to thank CNPq-Brazil (Bolsa de Produtividade, grant 303733/2017-
254 9) for financial support.

255

256

257

258 **Tables**

259

260 **Table 1:** Patient characteristics

	Alzheimer's disease	Healthy control
Number of cases		
	111	173
Age		
<65	60/111	90/173
≥65	51/111	79/173
Unknown	-	4/173
Gender		
Female	50/111	103/173
Male	61/111	68/173
Unknown	-	2/173

261

262

263

264

265

266

267

268

269

270

271 **Table 2:** Quality parameters for PCA-QDA model. PPV: positive predictive value, NPV:
272 negative predictive value.

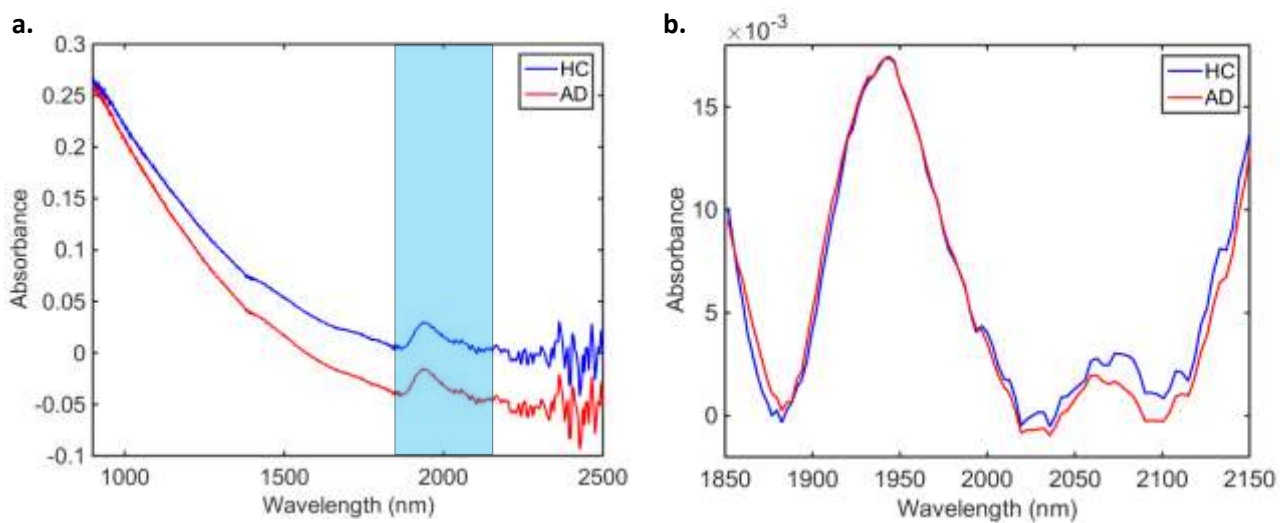
Parameter	Value (%)
Accuracy	92.8
Sensitivity	87.5
Specificity	96.1
PPV	93.3
NPV	92.5

273

274

275

276 **Figures**

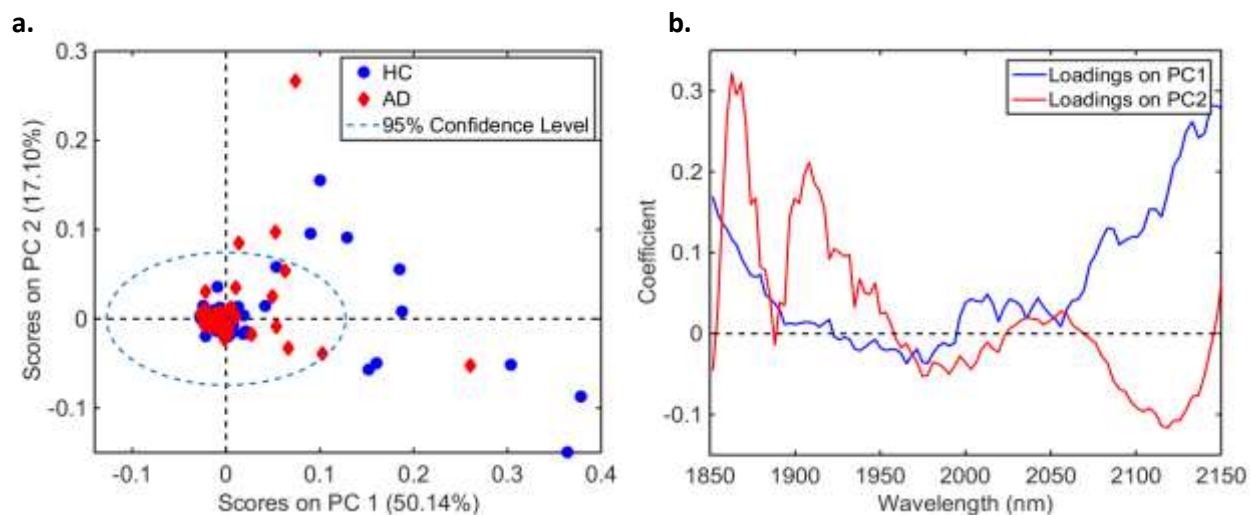


277

278 **Figure 1.** Average (a) raw and (b) pre-processed NIR spectra for healthy controls (HC) and
279 Alzheimer's disease (AD) patients.

280

281

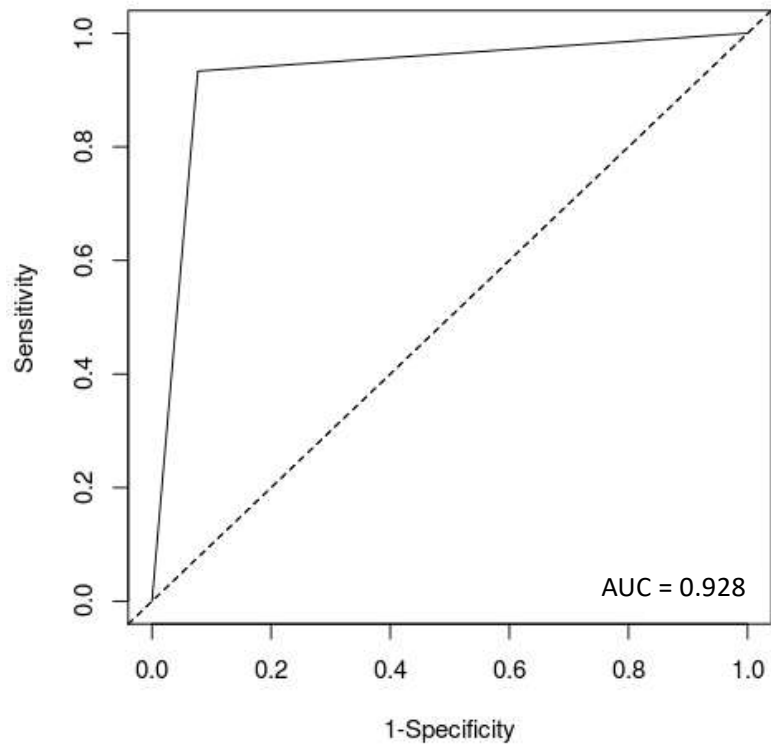


282

283 **Figure 2.** (a) PCA scores on PC1 and PC2 for healthy controls (HC) and Alzheimer's disease
 284 (AD) samples (explained variance for each PC inside parenthesis); (b) PCA loadings based on
 285 PC1 and PC2.

286

287



288

289 **Figure 3.** ROC curve for PCA-QDA model. AUC stands for area under the curve.

290

291

292

293

294

295

296

297

298 **References**

299 1. Policy Brief for Head of Government, *Alzheimer's Disease International*
300 (<https://www.alz.co.uk/research/GlobalImpactDementia2013.pdf>).

301 2. P. Martin, W. Anders, G. Maëlenn, A. Gemma-Claire, W. Yu-Tzu and P. Matthew, *World*
302 *Alzheimer Report 2015: the global impact of dementia: an analysis of prevalence, incidence,*
303 *cost and trends*, Alzheimer's Disease International, 2015.
304 (<https://www.alz.co.uk/research/WorldAlzheimerReport2015.pdf>).

305 3. L. Wang and B. Mizaikoff, *Anal Bioanal Chem*, 2008, **391**, 1641-1654.

306 4. D. I. Ellis and R. Goodacre, *Analyst*, 2006, **131**, 875-885.

307 5. G. Reich, *Adv Drug Del Rev*, 2005, **57**, 1109-1143.

308 6. A. Sakudo, *Clin Chim Acta*, 2016, **455**, 181-188.

309 7. R. K. Lauridsen, H. Everland, L. F. Nielsen, S. B. Engelsen and L. Nørgaard, *Skin Res Technol*,
310 2003, **9**, 137-146.

311 8. G. Pichler, B. Urlsberger, P. Jirak, H. Zotter, E. Reiterer, W. Müller and M. Borkenstein,
312 *Diabetes Care*, 2004, **27**, 1942-1946.

313 9. M. K. Simick, R. A. Jong, B. C. Wilson and L. D. Lilge, *J Biomed Opt*, 2004, **9**, 794-804.

314 10. H. Chen, Z. Lin, L. Mo, T. Wu and C. Tan, *Biomed Res Int*, 2015, **2015**.

315 11. D. H. Burns, S. Rosendahl, D. Bandilla, O. C. Maes, H. M. Chertkow and H. M. Schipper, *J*
316 *Alzheimers Dis*, 2009, **17**, 391-397.

317 12. A. Sakudo, H. Kuratsune, Y. H. Kato and K. Ikuta, *Clin Chim Acta*, 2012, **413**, 1629-1632.

318 13. M. Paraskevaidi, P. L. Martin-Hirsch and F. L. Martin, *Mol Neurodegener*, 2018, **13**, 20.

319 14. P. Carmona, M. Molina, M. Calero, F. Bermejo-Pareja, P. Martinez-Martin and A. Toledano, *J*
320 *Alzheimers Dis*, 2013, **34**, 911-920.

321 15. E. Ryzhikova, O. Kazakov, L. Halamkova, D. Celmins, P. Malone, E. Molho, E. A. Zimmerman
322 and I. K. Lednev, *J Biophotonics*, 2015, **8**, 584-596.

323 16. R. Michael, A. Lenferink, G. F. Vrensen, E. Gelpi, R. I. Barraquer and C. Otto, *Sci Rep*, 2017, **7**,
324 15603.

325 17. M. Griebel, M. Daffertshofer, M. Stroick, M. Syren, P. Ahmad-Nejad, M. Neumaier, J. Backhaus,
326 M. G. Hennerici and M. Fatar, *Neurosci Lett*, 2007, **420**, 29-33.

327 18. M. Grimbergen, C. van Swol, R. van Moorselaar, J. Uff, A. Mahadevan-Jansen and N. Stone, *J*
328 *Photochem Photobiol B: Biol*, 2009, **95**, 170-176.

329 19. B. W. De Jong, T. C. Bakker Schut, K. Maquelin, T. van der Kwast, C. H. Bangma, D.-J. Kok and
330 G. J. Puppels, *Anal Chem*, 2006, **78**, 7761-7769.

331 20. L. Mikoliunaite, R. D. Rodriguez, E. Sheremet, V. Kolchuzhin, J. Mehner, A. Ramanavicius and
332 D. R. Zahn, *Sci Rep*, 2015, **5**, 13150.

333 21. J. De Meutter, K.-M. Derfoufi and E. Goormaghtigh, *Biomed Spectrosc Imaging*, 2016, **5**, 145-
334 154.

335 22. M. J. Pilling, P. Bassan and P. Gardner, *Analyst*, 2015, **140**, 2383-2392.

336 23. L. Cui, H. J. Butler, P. L. Martin-Hirsch and F. L. Martin, *Anal Methods*, 2016, **8**, 481-487.

337 24. M. J. Baker, J. Trevisan, P. Bassan, R. Bhargava, H. J. Butler, K. M. Dorling, P. R. Fielden, S. W.
338 Fogarty, N. J. Fullwood, K. A. Heys, C. Hughes, P. Lasch, P. L. Martin-Hirsch, B. Obinaju, G. D.
339 Sockalingum, J. Sulé-Suso, R. J. Strong, M. J. Walsh, B. R. Wood, P. Gardner and F. L. Martin,
340 *Nat Protoc*, 2014, **9**, 1771-1791.

341 25. R. W. Kennard and L. A. Stone, *Technometrics*, 1969, **11**, 137-148.

342 26. R. Bro and A. K. Smilde, *Anal Methods*, 2014, **6**, 2812-2831.

343 27. C. L. Morais and K. M. Lima, *J Braz Chem Soc*, 2017, **31**.

344 28. S. J. Dixon and R. G. Brereton, *Chemom Intellig Lab Syst*, 2009, **95**, 1-17.

345 29. J. Kuligowski, G. Quintás, C. Herwig and B. Lendl, *Talanta*, 2012, **99**, 566-573.

346 30. C. L. Morais and K. M. Lima, *Chemom Intellig Lab Syst*, 2017.

347 31. D. Goksuluk, S. Korkmaz, G. Zararsiz and A. E. Karaagaoglu, *R Journal*, 2016, **8**, e30.

- 348 32. J. J. Workman Jr, *Appl Spectrosc Rev*, 1996, **31**, 251-320.
- 349 33. S. Türker-Kaya and C. W. Huck, *Molecules*, 2017, **22**, 168.
- 350 34. M. Manley, *Chem Soc Rev*, 2014, **43**, 8200-8214.
- 351 35. A. Hye, S. Lynham, M. Thambisetty, M. Causevic, J. Campbell, H. L. Byers, C. Hooper, F. Rijdsdijk,
352 S. J. Tabrizi, S. Banner, C. E. Shaw, C. Foy, M. Poppe, N. Archer, G. Hamilton, J. Powell, R. G.
353 Brown, P. Sham, M. Ward and S. Lovestone, *Brain*, 2006, **129**, 3042-3050.
- 354 36. S. Ray, M. Britschgi, C. Herbert, Y. Takeda-Uchimura, A. Boxer, K. Blennow, L. F. Friedman, D.
355 R. Galasko, M. Jutel and A. Karydas, *Nat Med*, 2007, **13**, 1359.
- 356 37. B. Olsson, R. Lautner, U. Andreasson, A. Öhrfelt, E. Portelius, M. Bjerke, M. Hölttä, C. Rosén,
357 C. Olsson and G. Strobel, *Lancet Neurol*, 2016, **15**, 673-684.
- 358 38. N. Mattsson, U. Andreasson, H. Zetterberg, K. Blennow and I. for the Alzheimer's Disease
359 Neuroimaging, *JAMA Neurol*, 2017, **74**, 557-566.
- 360 39. N. Mattsson, H. Zetterberg, S. Janelidze, P. S. Insel, U. Andreasson and E. Stomrud, *Neurology*,
361 2016, **87**.
- 362 40. M. Mapstone, A. K. Cheema, M. S. Fiandaca, X. Zhong, T. R. Mhyre, L. H. MacArthur, W. J. Hall,
363 S. G. Fisher, D. R. Peterson, J. M. Haley, M. D. Nazar, S. A. Rich, D. J. Berlau, C. B. Peltz, M. T.
364 Tan, C. H. Kawas and H. J. Federoff, *Nat Med*, 2014, **20**, 415-418.
- 365 41. A. Nakamura, N. Kaneko, V. L. Villemagne, T. Kato, J. Doecke, V. Doré, C. Fowler, Q.-X. Li, R.
366 Martins and C. Rowe, *Nature*, 2018, **554**, 249.
- 367 42. M. Paraskevasidi, C. L. Morais, K. M. Lima, J. S. Snowden, J. A. Saxon, A. M. Richardson, M.
368 Jones, D. M. Mann, D. Allsop and P. L. Martin-Hirsch, *Proc Natl Acad Sci USA*, 2017, 201701517.
- 369 43. E. Peuchant, S. Richard-Harston, I. Bourdel-Marchasson, J. F. Dartigues, L. Letenneur, P.
370 Barberger-Gateau, S. Arnaud-Dabernat and J. Y. Daniel, *Transl Res*, 2008, **152**, 103-112.
- 371 44. S. Mordechai, E. Shufan, B. P. Katz and A. Salman, *Analyst*, 2017, **142**, 1276-1284.
- 372 45. P. Carmona, M. Molina, E. López-Tobar and A. Toledano, *Anal Bioanal Chem*, 2015, **407**, 7747-
373 7756.
- 374 46. M. Paraskevasidi, C. L. Morais, D. E. Halliwell, D. M. Mann, D. Allsop, P. L. Martin-Hirsch and F.
375 L. Martin, *ACS Chem Neurosci*, 2018.